A Study of Multistep Model Predictive Direct Current Control for Dynamic Drive Applications with High Switching Frequency

Zheng Hu, Qian Liu and Kay Hameyer*

**Institute of Electrical Machines, RWTH Aachen University, Germany, zheng.hu@iem.rwth-aachen.de*

Keywords: multistep direct MPC, integer least-square, sphere decoding, predictive control.

Abstract

In this work a study of multistep model predictive direct current control in high switching frequency range will be presented. The optimization problem underlying this control approach is represented by an integer least-square problem, which can be solved by the sphere decoding algorithm. In this paper, the system performance, both in transient and steady-state will be analysed in such a way, that a direct current controller can be obtained for an induction motor operated by a two-level voltage source inverter in high dynamic drive applications, which achieves higher dynamics when compared to the classic modulation based schemes and lower current distortion than other direct control approaches.

1 Introduction

Since the last decades the direct predictive control has become an alternative technology to the conventional pulse width modulation (PWM) based approaches for power electronics. Instead of defining the duty cycle, the switch positions of the inverter can be directly manipulated, which means no modulator is required. Depending on the applications, control strategies adressing different objectives are proposed, among which direct torque control (DTC) and direct current control (DCC) are the most prominent representatives.

DTC is nowadays a well-established industrial standard. By selecting an optimal inverter switch combination from the switching table according to derivation of torque and flux linkage, the stator flux vector is driven to the desired position. Despite its simplicity, DTC features rapid and accurate dynamic torque responses throughout the entire operating range, and is robust with respect to motor parameters and perturbations [1]. On the other hand, the main disadvantages of DTC are the notable current and torque ripple as well as its variable switching frequency behavior [2]. DCC scheme can be deemed as an adaptation of DTC, in the sense that it is by analogy with DTC in terms of principle and implementation despite the control objectives of DCC are transformed into producing desired three-phase load current. The basic principle of DCC is to select the proper stator voltage vector such that the stator current vector is kept within a hysteresis bound moving with time.

With the development of microprocessor techniques the model predictive control (MPC) has recently been more and more popular in the field power electronics [3, 4]. The most widely used MPC approaches are finite-control-set MPC (FCS-MPC) based on the enumeration / exhaustive search algorithm according to the underlying minimization problem of the objective function [5–11]. Therefore, such approaches take exponential computational effort with increasing length of the prediction horizon. This is the reason why the prediction step size is usually limited to one or two. The distortion of these approaches is commonly higher than that of the modulation schemes. In [12], an extrapolation strategy is proposed, in which a switching horizon and a prediction horizon are defined. The basic idea is to compute input sequences over the switching horizon that is significantly shorter than the prediction horizon, which is determined by linearly extrapolating the promising state trajectory within their constraints. In such a way, a multistep direct MPC can be obtained with modest computational complexity. However, the accuracy is compromised.

In [13], a novel multistep direct MPC approach is introduced by definition of a constrained finite-time optimal control problem (CFTOC). The optimization problem is formulated into an integer least-squares (ILS) problem solved by the sphere-decoding algorithm introduced in [14]. The approach was implemented on a medium-voltage induction machine fed by a three-level voltage source inverter (VSI). The focus was mainly on the steady-state performance for the switching frequency range between 200Hz and 350Hz. The performance evaluation is given in [15]. Based on this concept, the application for two-level VSI and high switching frequency range, which is commonly used in the high dynamic electrical drive systems, is studied in this paper. Both the dynamic and steady-state performance will be compared to the space vector modulation (SVM) and enumeration-based FCS-MPC.

2 Prediction Model

In this section the discrete-time models of drive systems, that is induction motors (IM) driven by two-level three-phase voltage source inverter (VSI), will be derived. More Specifically, the model should capture the hybrid nature of the DCC drive system, i.e. a system incorporating both continuous and discrete

variables, in particular binary manipulated control variables.

By means of the power-invariant Park transformation, the three-phase system is transformed into the $\alpha\beta$ reference frame by

$$\begin{aligned} \boldsymbol{\xi}_{\alpha\beta} &= \tilde{\boldsymbol{P}}\boldsymbol{\xi}_{abc} \quad \text{with} \\ \tilde{\boldsymbol{P}} &= \sqrt{\frac{2}{3}}\begin{bmatrix} 1 & \frac{1}{2} & -\frac{1}{2} \\ 0 & \frac{\sqrt{3}}{2} & -\frac{\sqrt{3}}{2} \end{bmatrix}, \end{aligned} \tag{1}$$

where $\boldsymbol{\xi}_{abc} = [\xi_a \xi_b \xi_c]^T$ and $\boldsymbol{\xi}_{\alpha\beta} = [\xi_\alpha \xi_\beta]^T$ denote the parameter vector from the three-phase system and in the $\alpha\beta$ reference frame, respectively.

The VSI is capable to produce at each phase two voltage levels, either $\frac{V_{dc}}{2}$ or $\frac{-V_{dc}}{2}$, assuming that the DC-link voltage is constant and the neutral point potential u_{np} is fixed. Let integer variables u_a,u_b and $u_c \in \mathcal{U}$ denote the switching state of each phase, where

$$\mathcal{U} \triangleq \{1, -1\} \tag{2}$$

is the single-phase constraint set. The elements 1 and -1 correspond to the phase voltages $\frac{V_{dc}}{2}$ or $\frac{-V_{dc}}{2}$ respectively. Therefore, the switching state vector $\boldsymbol{u}_{abc} = [u_a\ u_b\ u_c]^T$ applied to the inverter at certain time instance is selected from a 2^3-element finite set defined as triple Cartesian product of the set $\mathcal{U}$

$$\boldsymbol{\mathcal{U}} \triangleq \mathcal{U} \times \mathcal{U} \times \mathcal{U}. \tag{3}$$

Accordingly, the voltage applied to the machine terminals in orthogonal coordinates can be obtained via

$$\boldsymbol{u}_{\alpha\beta} = \frac{V_{dc}}{2}\tilde{\boldsymbol{P}}u_{abc}. \tag{4}$$

The dynamics of the induction motor is modeled in $\alpha\beta$ reference frame. The state space equations of the continuous-time system are given by

$$\begin{aligned} \dot{\boldsymbol{x}}(t) &= \boldsymbol{F}\boldsymbol{x}(t) + \boldsymbol{G}\boldsymbol{u}_{\alpha\beta}(t) \\ \boldsymbol{y}(t) &= \boldsymbol{C}\boldsymbol{x}(t), \end{aligned} \tag{5}$$

where the state, input and output vectors are defined as

$$\begin{aligned} \boldsymbol{x} &= [i_{s\alpha} \quad i_{s\beta} \quad \psi'_{r\alpha} \quad \psi'_{r\beta}]^T \\ \boldsymbol{u}_{\alpha\beta} &= [u_\alpha \quad u_\beta]^T \\ \boldsymbol{y} &= [i_{s\alpha} \quad i_{s\beta}]^T. \end{aligned} \tag{6}$$

The symbols i_s and ψ_r represent the stator current and the rotor flux, respectively. The system matrices $\boldsymbol{F}$, $\boldsymbol{G}$ and $\boldsymbol{C}$ are described in the following respective forms

$$\boldsymbol{F} = \begin{bmatrix} -\frac{1}{\tau_s} & 0 & \frac{L_m}{\tau_r D} & \frac{w_r L_m}{D} \\ 0 & -\frac{1}{\tau_s} & -\frac{w_r L_m}{D} & \frac{L_m}{\tau_r D} \\ \frac{L_m}{\tau_r} & 0 & -\frac{1}{\tau_r} & -\omega_r \\ 0 & \frac{L_m}{\tau_r} & \omega_r & -\frac{1}{\tau_r} \end{bmatrix}, \tag{7a}$$

$$\boldsymbol{G} = \frac{L'_r}{D}\frac{V_{dc}}{2}\begin{bmatrix} 1 & 0 \\ 0 & 1 \\ 0 & 0 \\ 0 & 0 \end{bmatrix}, \tag{7b}$$

$$\boldsymbol{C} = \begin{bmatrix} 1 & 0 & 0 & 0 \\ 0 & 1 & 0 & 0 \end{bmatrix}. \tag{7c}$$

The notations τ_s, τ_r and D are defined as

$$\tau_s = \frac{L'_r D}{R_s {L'_r}^2 + L'_r L_m^2}, \tag{8a}$$

$$\tau_r = \frac{L'_r}{R_r}, \tag{8b}$$

$$D = L_s L'_r - L_m^2. \tag{8c}$$

By means of Euler Forward Method, the discrete-time model can be obtained in the following formulation

$$\begin{aligned} \boldsymbol{x}(k+1) &= \boldsymbol{A}\boldsymbol{x}(k) + \boldsymbol{B}\tilde{\boldsymbol{P}}\boldsymbol{u}_{abc}(k) \\ \boldsymbol{y}(k) &= \boldsymbol{C}(k). \end{aligned} \tag{9}$$

The discrete-time system and input matrices are given by

$$\boldsymbol{A} = \boldsymbol{I} + \boldsymbol{F}T_s \tag{10}$$

$$\boldsymbol{B} = \frac{V_{dc}}{2}\boldsymbol{G}T_s, \tag{11}$$

where $\boldsymbol{I}$ is the identity matrix of appropriate dimensions, which in this case is 4×4, and T_s denotes the sampling time.

3 Optimization Control Problem

In this section, the optimization problem of the multi-step model predictive direct current controller is presented.

3.1 Constrained Finite-Time Optimal Control Problem

The objective function of the optimal control problem is formulated by

$$J = \sum_{l=k}^{k+N-1} \|\boldsymbol{i}_{\alpha\beta,error}(l+1)\|_2^2 + \lambda_u \|\Delta\boldsymbol{u}(l)\|_2^2, \tag{12}$$

where $\boldsymbol{i}_{\alpha\beta,error}(l) = \boldsymbol{i}_{\alpha\beta,ref}(l) - \boldsymbol{i}_{\alpha\beta}(l)$ and $\Delta\boldsymbol{u}(l) = \boldsymbol{u}_{abc}(l) - \boldsymbol{u}_{abc}(l-1)$. The weighting factor λ_u penalizes the switching transitions and adjusts the trade-off between tracking error and switching effort. After introducing the switching sequence over the prediction horizon at time instant k

$$\boldsymbol{U}(k) = \left[\boldsymbol{u}(k)^T \quad \boldsymbol{u}(k+1)^T, ..., \boldsymbol{u}(k+N-1)^T\right]^T \tag{13}$$

the CFTOC problem can be compacted as

$$\begin{aligned} \min_{U(k)} \quad & J(\boldsymbol{x}(k), \boldsymbol{u}(k-1), \boldsymbol{U}(k), \boldsymbol{y}_{ref}(k)) \\ \text{s.t.} \quad & \text{Equation (9)}\ , \boldsymbol{U}(k) \in \mathbb{U}, \end{aligned} \tag{14}$$

where $\mathbb{U} \triangleq \boldsymbol{\mathcal{U}} \times \cdots \times \boldsymbol{\mathcal{U}}$ is the N-times Cartesian product of the set $\boldsymbol{\mathcal{U}}$, and $\boldsymbol{\mathcal{U}}$ denotes the set of discrete three-phase switching states as aforementioned.

As the 2-norm is used in the objective function, the on-line solving of CFTOC problem (14) amounts either to obtaining

the optimal switching state via enumeration, which features one-by-one exhaustive search through tentative candidate set and is far from being efficient, or to solving a mixed-integer quadratic problem (MIQP), for which efficient off-the-shelf solvers such as CPLEX and GUROBI exist. However, such approach does not take advantage of the particular structure of the CFTOC problem and the receding horizon policy adopted by MPC.

3.2 Integer Least-Squares Problem

In fact, the CFTOC problem (14) highly resembles Integer Least-squares (ILS) problems in the way that they both search for the vector with integer entries that minimizes a certain objective function. This distinguishing feature can be exploited to greatly reduce the computational burden, thus enabling the implementation of long prediction horizon. The general form of the ILS problem is

$$\min_{s\in\mathcal{Z}^m} \quad \|\boldsymbol{x}-\boldsymbol{H}\boldsymbol{s}\|_2^2\,, \tag{15}$$

where $x \in \mathcal{R}^{n\times 1}, \boldsymbol{H} \in \mathcal{R}^{n\times m}$, $\mathcal{Z}^m$ denotes the m-dimensional vector with integer entries. However, the search space is often restricted to a finite subset $\mathcal{D} \subset \mathcal{Z}^m$, which yields an ILS problem subject to finite alphabet (FA) constraints

$$\min_{s\in\mathcal{D}\subset\mathcal{Z}^m} \quad \|\boldsymbol{x}-\boldsymbol{H}\boldsymbol{s}\|_2^2\,. \tag{16}$$

The ILS problem has a simple geometric interpretation. As the entries of $\boldsymbol{s}$ run over the integers, $\boldsymbol{s}$ spans the rectangular m-dimensional lattice $\mathcal{Z}^m$. The matrix $\boldsymbol{H}$ is known as *lattice-generating matrix*, and its columns represent m linearly independent vectors that generate a lattice, i.e. the set of all linear combinations of the basis vectors $\boldsymbol{h}_i$

$$\mathcal{L}(\boldsymbol{H}) = \{\sum_{i=1}^{m} w_i\boldsymbol{h}_i | w_i \in \mathbb{Z}\}\,. \tag{17}$$

However, for any given $\boldsymbol{H}$, the n-dimensional vector $\boldsymbol{H}\boldsymbol{s}$ spans a skewed lattice compared to the integer lattice (see Fig. 1). Therefore, given the skewed lattice $\boldsymbol{H}\boldsymbol{s}$ and given a vector $\boldsymbol{x} \in \mathcal{R}^{n\times 1}$, the ILS problem amounts to finding the closest lattice point to $\boldsymbol{x}$. Generally speaking, the ILS problem is NP-hard both in worst-case sense [16] and in average sense [17], however efficient algorithms abound for solving the ILS problem.

3.3 Reformulation of the CFTOC Problem

Motivated by the fact that efficient algorithms can be adapted to solving the ILS problem, the CFTOC problem (14) is reformulated into an ILS problem by techniques introduced in [13] in the sequel. We define the output sequence $\boldsymbol{Y}(k)$ as

$$\boldsymbol{Y}(k) = [\boldsymbol{y}^T(k+1), ..., \boldsymbol{y}^T(k+N)]^T \tag{18}$$

and the output reference sequence $\boldsymbol{Y}_{ref}(k)$ is defined accordingly. The output sequence can be then described by

$$\boldsymbol{Y}(k) = \boldsymbol{\Gamma}\boldsymbol{x}(k) + \boldsymbol{\Upsilon}\boldsymbol{U}(k), \tag{19}$$

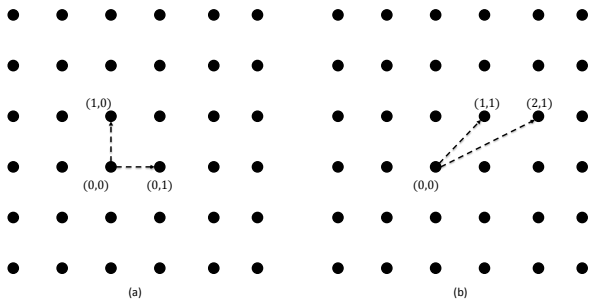

Fig. 1: Two-dimensional lattice generated by two different bases.

where the two matrices are defined as

$$\boldsymbol{\Gamma} = \begin{bmatrix}\boldsymbol{C}\boldsymbol{A} & \boldsymbol{C}\boldsymbol{A}^2 & \dots & \boldsymbol{C}\boldsymbol{A}^N\end{bmatrix}^T, \tag{20a}$$

$$\boldsymbol{\Upsilon} = \begin{bmatrix}\boldsymbol{C}\boldsymbol{B}\tilde{\boldsymbol{P}} & \boldsymbol{0} & ... & \boldsymbol{0}\\ \boldsymbol{C}\boldsymbol{A}\boldsymbol{B}\tilde{\boldsymbol{P}} & \boldsymbol{C}\boldsymbol{B}\tilde{\boldsymbol{P}} & ... & \boldsymbol{0}\\ \boldsymbol{C}\boldsymbol{A}^{N-1}\boldsymbol{B}\tilde{\boldsymbol{P}} & \boldsymbol{C}\boldsymbol{A}^{N-2}\boldsymbol{B}\tilde{\boldsymbol{P}} & ... & \boldsymbol{0}\end{bmatrix}. \tag{20b}$$

Therefore, the objective function (12) can be rewritten in a compact form

$$J = \theta(k) + 2(\boldsymbol{\Theta}(k))^T\boldsymbol{U}(k) + \boldsymbol{U}^T(k)\boldsymbol{Q}\boldsymbol{U}(k) \tag{21}$$

with

$$\theta(k) \triangleq \|\boldsymbol{\Gamma}\boldsymbol{x}(k) - \boldsymbol{Y}_{ref}(k)\|_2^2 + \lambda_u\|\boldsymbol{E}\boldsymbol{u}(k-1)\|_2^2 \tag{22a}$$

$$\boldsymbol{\Theta}(k) \triangleq ((\boldsymbol{\Gamma}\boldsymbol{x}(k) - \boldsymbol{Y}_{ref}(k))^T\boldsymbol{\Upsilon} - \lambda_u(\boldsymbol{E}\boldsymbol{u}(k-1))^T\boldsymbol{S})^T \tag{22b}$$

$$\boldsymbol{Q} \triangleq \boldsymbol{\Upsilon}^T\boldsymbol{\Upsilon} + \lambda_u\boldsymbol{S}^T\boldsymbol{S}, \tag{22c}$$

where

$$\boldsymbol{S} = \begin{bmatrix}\boldsymbol{I} & \boldsymbol{0} & ... & \boldsymbol{0}\\ -\boldsymbol{I} & \boldsymbol{I} & ... & \boldsymbol{0}\\ \boldsymbol{0} & -\boldsymbol{I} & ... & \boldsymbol{0}\\ \vdots & \vdots & & \vdots\\ \boldsymbol{0} & \boldsymbol{0} & ... & \boldsymbol{I}\end{bmatrix}, \tag{23a}$$

$$\boldsymbol{E} = \begin{bmatrix}\boldsymbol{I} & \boldsymbol{0} & \boldsymbol{0} & \dots & \boldsymbol{0}\end{bmatrix}^T. \tag{23b}$$

By expanding the squared Euclidean norm (21) can be rewritten into

$$J = (\boldsymbol{U}(k) + \boldsymbol{Q}^{-1}\boldsymbol{\Theta}(k))^T\boldsymbol{Q}(\boldsymbol{U}(k) + \boldsymbol{Q}^{-1}\boldsymbol{\Theta}(k)) + const(k). \tag{24}$$

Would the integral constraints on $\boldsymbol{U}(k)$ be ignored, The unconstrained optimal solution to (24) amounts to

$$\boldsymbol{U}_{unc}(k) = -\boldsymbol{Q}^{-1}\boldsymbol{\Theta}(k). \tag{25}$$

Inserting (25) into (24), the objective function can be rewritten into

$$J = (\boldsymbol{U}(k) - \boldsymbol{U}_{unc}(k))^T\boldsymbol{Q}(\boldsymbol{U}(k) - \boldsymbol{U}_{unc}(k)) + const(k). \tag{26}$$

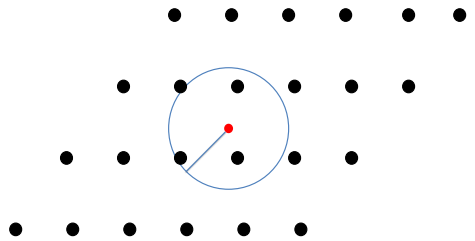

Fig. 2: Geometric interpretation of SD algorithm.

Since $\boldsymbol{Q}$ is symmetric and positive definite for $\lambda_u > 0$, there exists a unique invertible and lower triangular matrix $\boldsymbol{H}$ which satisfies

$$\boldsymbol{H}^T\boldsymbol{H} = \boldsymbol{Q}. \tag{27}$$

$\boldsymbol{H}$ can be obtained by Cholesky decomposition of $\boldsymbol{Q}^{-1}$ which is also positive definite noting that the $\boldsymbol{H}^{-1}$ is also lower triangular hence

$$\boldsymbol{H}^{-1}\boldsymbol{H}^{-T} = \boldsymbol{Q}^{-1}. \tag{28}$$

Then we define

$$\bar{\boldsymbol{U}}_{unc}(k) \triangleq \boldsymbol{H}\boldsymbol{U}_{unc}(k). \tag{29}$$

By substituting (27) and (29) ,the objective function (26) can be rewritten into

$$J = (\boldsymbol{H}\boldsymbol{U}(k) - \bar{\boldsymbol{U}}_{unc}(k))^T(\boldsymbol{H}\boldsymbol{U}(k) - \bar{\boldsymbol{U}}_{unc}(k)) + const(k). \tag{30}$$

Noting that the constant term is independent of $\boldsymbol{U}(k)$, therefore the CFTOC problem (14) is finally reformulated into an ILS problem (15)

$$\begin{aligned} \min_{\boldsymbol{U}(k)} \quad & \|\boldsymbol{H}\boldsymbol{U}(k) - \bar{\boldsymbol{U}}_{unc}(k)\|_2^2 \\ \text{s.t.} \quad & \text{Equation (9)}, \boldsymbol{U}(k) \in \mathbb{U}. \end{aligned} \tag{31}$$

3.4 Sphere Decoding Algorithm

As aforementioned, abundant existing algorithms have enabled the efficient solving of ILS problems, and sphere decoding (SD) algorithm is one of the most prominent representatives. In the following the principle of SD algorithm is briefly introduced. Although SD algorithms employ different notations, they shared a common principle that is quite intuitive as illustrated in Fig. 2. Instead of searching all valid points in the lattice to find the one which minimizes the objective function (15), SD attempts to restrict the search region to a sphere of radius ρ centered around the given vector $\boldsymbol{x}$, i.e.

$$\|\boldsymbol{x} - \boldsymbol{H}\boldsymbol{s}\|_2^2 \leq \rho^2, \tag{32}$$

thereby significantly reducing the computational burden, and the complexity is demonstrated in [14, 18].

The ILS formulation (31) of the original CFTOC problem boils down to finding the lattice point $\boldsymbol{U}(k)$ that lies within a sphere centered at $\bar{\boldsymbol{U}}_{unc}(k)$ of initial radius $\rho(k) > 0$. Eventually the optimal solution $\boldsymbol{U}_{opt}(k)$ has the shortest Euclidean distance to the sphere center among all the candidate switching sequences. A SD algorithm tailored from the one proposed in [19] is employed in our case studied which exploits the fact that $\boldsymbol{U}$ features finite set elements:

$$\|\boldsymbol{H}\boldsymbol{U}(k) - \bar{\boldsymbol{U}}_{unc}(k)\|_2^2 \leq \rho^2(k). \tag{33}$$

The property of $\boldsymbol{H}$ being a lower-triangular matrix now comes in handy. By expanding the quadratic norm 33, we obtain

$$\rho^2 \geq (\bar{U}_1 - H_{1,1}U_1)^2 + (\bar{U}_2 - H_{2,1}U_1 - H_{2,2}U_2)^2 + \cdots, \tag{34}$$

where the subscript *unc* of $\bar{\boldsymbol{U}}_{unc}$ and the time instant k is omitted for simplicity reason.

There are only two possible switching states of each phase, which implies that two branches stretch out from each node. Starting from the first layer, the left node -1 is visited. The current Euclidean distance d' is given by

$$d'^2 = d_1^2 \triangleq (\bar{U}_1 - H_{1,1}U_1)^2. \tag{35}$$

Then evaluating

$$\rho^2 \geq d'^2 \tag{36}$$

if the condition holds, which means -1 is inside the sphere, the search proceeds to the next layer hitting firstly the left node -1. The current Euclidean distance is updated by simply adding a term to the previously calculated d_1^2, i.e.

$$d'^2 = d_1^2 + (\bar{U}_2 - H_{2,1}U_1 - H_{2,2}U_2)^2. \tag{37}$$

The first candidate switching sequence $\boldsymbol{U} = [-1\ -1\ -1]^T$ is then obtained when the last layer has been reached. Its associated squared distance which is less or equal to the initial radius is now adopted as the new radius of the sphere, implying the search space shrinks, which is denoted as shrining-radius strategy. Subsequently we explore the second node of the third layer, which turns out to be beyond the sphere. Since all the two branches that stem from the left node of second layer are run through, we move on to the right node 1, whose distance however exceeds the radius, then a certificate is given to the node and all its associated branches that it provides only suboptimal solutions, i.e., solutions that are worse than the incumbent optimum $\boldsymbol{U} = [-1 -1 -1]^T$. Therefore, the search in this path can be pruned. This feature distinguishes SD algorithm from the conventional enumeration approach (see Fig. 3a). The above described tree search is depicted in Fig. 3b, where black solid circles denote nodes that are explored and verified to be inside the sphere, whereas the red ones indicate those beyond the sphere, the gray nodes are those which haven't been visited at all. The direction of the search process is indicated with black arrows. In summary, to find the optimal solution nodes are visited with a direction from left to right, and from layers of lower dimension to the ones of higher dimension unless reaching a dead end or full dimension where backtracking occurs.

Compared to the algorithm used in [13], the computational complexity of the algorithm in this work is further reduced by means of Schnorr- Euchner SD.

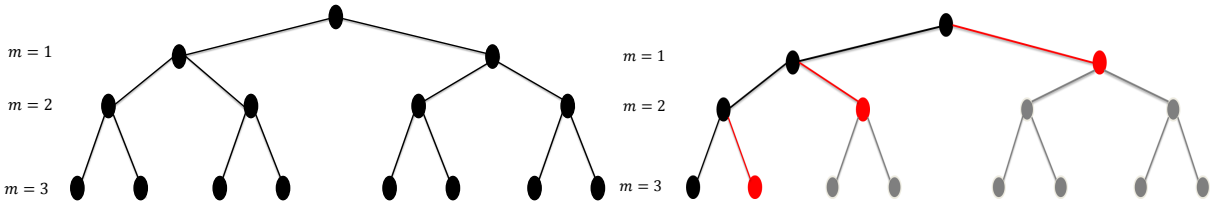

(a) Brute-force tree search employed in enumeration **(b)** Efficient tree search employed in SD algorithm

Fig. 3: Two typical tree search techniques for solving ILS problems.

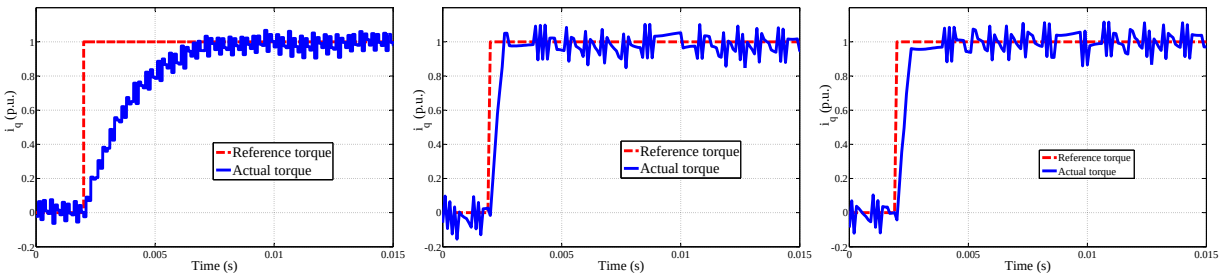

(a) Dynamic response of FOC with SVM **(b)** Dynamic response of enumeration-based FCS-MPC with $N = 1$ **(c)** Dynamic response of MSMPDCC with $N = 5$

Fig. 4: Dynamics during reference current steps for different approaches at $f_{sw} = 3000$Hz.

4 Simulation Results

Simulation results are presented in this chapter for evaluation of the multi-step model predictive direct current control (MSMPDCC) approach proposed in the previous section in terms of the dynamic and steady-state performance. In [13] it is introduced, the total harmonic distortion (THD) decreases generally with increasing switching frequency. Therefore, the weighting factor λ_u of MSMPDCC and FCS-MPC based on enumeration is tuned in such a way, that the same switching frequency is garanteed as the SVM approach. Fig. 4 shows the dynamic performance of Field Oriented Controller (FOC) based on PI and SVM, FCS-MPC based on enumeration with single prediction step and MSMPDCC with prediction step $N = 5$. The sampling frequency $f_s = 20$kHz and the switching frequency of the inverter $f_{sw} = 3$kHz.

Initially, the induction motor is running with a mechanical rotor speed of 800rpm under no-load operation, when the rotor flux which features the relatively slow dynamics settles to its steady-state value, a step from 0p.u. to 1p.u. in the quadrature current reference $i_{sq,ref}$ is imposed. It can be identified that the dynamical response of both FCS-MPC based on enumeration and MSMPDCC is far more prompt than that of SVM. The settling times of enumeration-based FCS-MPC and MSMPDCC are nearly identical. It is due to the fact that the voltage margins that are predominantly affected by the rotor speed are essentially the same. Regarding the steady-state performance, the current THD of the above three cases are computed via FFT analysis, which yields 4.335%, 6.505% and 6.121% respectively.

It can be concluded that during transient the length of prediction horizon has no profound impact on the dynamical performance of the MPDCC, which is on the contrary limited only by the available voltage. Generally, the MPDCC approach is superior to the conventional FOC with SVM in transient performance when featuring the same switching frequency of the inverter. However the steady performance of the proposed MPDCC approach is inferior to that of the SVM since for direct control scheme, voltage vector chosen from the hexagon is applied during the whole sampling interval. On the contrary, the SVM technique allows for a combination of the two adjacent active voltage vectors together with the inactive ones, which yields a smoother control action, therefore lower current THD.

Fig. 5 shows the relationship between THD and switching frequency as well as prediction horizon. In general, the $N = 1$ curve overlies the others at most of the switching frequencies. Therefore, the steady-state performance can be improved by increasing the prediction horizon, which is applicable by the MSMPDCC approach as aforementioned.

5 Conclusions

In this work the multistep direct current control approach is studied for the application in high switching frequency range. The original optimal problem is reformulated into an ILS problem. By incorporating an efficient sphere decoding algorithm, the computational burden is dramatically alleviated. Therefore, the implementation of a considerably long prediction

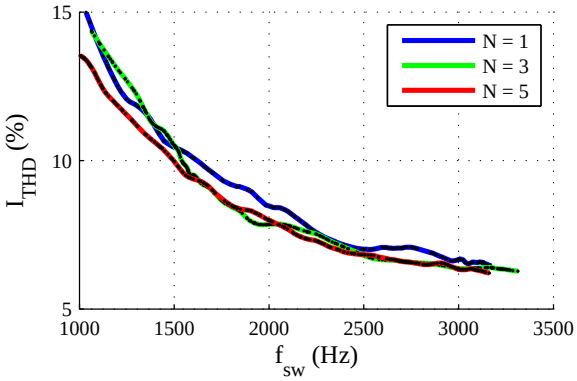

Fig. 5: I_{THD} as a function of f_{sw}.

horizon is possible. The long prediction horizon takes advantage of the high dynamic performance of the FCS-MPC and has a better steady-state performance compared to that of single prediction step.

References

[1] P. Tiitinen, P. Pohjalainen, and J. Lalu, "The next generation motor control method: Direct torque control (dtc)," *EPE Journal*, vol. 5, no. 1, pp. 14–18, 1995.

[2] D. Casadei, F. Profumo, G. Serra, and A. Tani, "Foc and dtc: two viable schemes for induction motors torque control," *IEEE Transactions on Power Electronics*, vol. 17, no. 5, pp. 779–787, 2002.

[3] J. Maciejowski, *Predictive control with constraints*. Prentice Hall, 2002.

[4] D. Q. M. James B. Rawlings, *Model Predictive Control: Theory and Design*. WI: Nob Hill, 2009.

[5] J. Rodríguez, J. Pontt, C. A. Silva, P. Correa, P. Lezana, P. Cortés, and U. Ammann, "Predictive Current Control of a Voltage Source Inverter," *IEEE Transactions on Industrial Electronics*, vol. 54, no. 1, pp. 495–503, Feb 2007.

[6] P. Cortés, M. P. Kazmierkowski, R. Kennel, D. E. Quevedo, and J. Rodríguez, "Predictive Control in Power Electronics and Drives," *IEEE Transactions on Industrial Electronics*, vol. 55, no. 12, pp. 4312–4324, Dec 2008.

[7] S. Kouro, P. Cortés, R. Vargas, U. Ammann, and J. Rodríguez, "Model Predictive ControlA Simple and Powerful Method to Control Power Converters," *IEEE Transactions on Industrial Electronics*, vol. 56, no. 6, pp. 1826–1838, June 2009.

[8] H. Miranda, P. Cortes, J. I. Yuz, and J. Rodriguez, "Predictive Torque Control of Induction Machines Based on State-Space Models," *IEEE Transactions on Industrial Electronics*, vol. 56, no. 6, pp. 1916–1924, June 2009.

[9] S. Alireza Davari, D. Khaburi, F. Wang, and R. Kennel, "Using full order and reduced order observers for robust sensorless predictive torque control of induction motors," *Power Electronics, IEEE Transactions on*, vol. 27, no. 7, pp. 3424–3433, July 2012.

[10] J. Rodriguez, M. P. Kazmierkowski, J. R. Espinoza, R. Zanchetta, H. Abu-Rub, H. A. Young, and C. A. Rojas, "State of the Art of Finite Control Set Model Predictive Control in Power Electronics," *IEEE Transactions on Industrial Informatics*, vol. 9, no. 2, pp. 1003–1016, May 2013.

[11] E. Fuentes, D. Kalise, J. Rodriguez, and R. Kennel, "Cascade-Free Predictive Speed Control for Electric Drives," *IEEE Transactions on Industrial Electronics*, vol. 61, no. 5, pp. 2176–2184, May 2014.

[12] T. Geyer, G. Papafotiou, and M. Morari, "Model Predictive Control in Power Electronics : A Hybrid Systems Approach," in *Decision and Control, 2005 European Control Conference, CDC-ECC '05. 44th IEEE Conference on*, Seville, Spain, Dec 2005, pp. 5606–5611.

[13] T. Geyer and D. E. Quevedo, "Multistep direct model predictive control for power electronics - Part 1: Algorithm," in *Energy Conversion Congress and Exposition (ECCE)*, Denver, CO, Sept. 2013, pp. 1154–1161.

[14] B. Hassibi and H. Vikalo, "On the sphere-decoding algorithm I. Expected complexity," *Signal Processing, IEEE Transactions on*, vol. 53, no. 8, pp. 2806–2818, 2005.

[15] T. Geyer and D. E. Quevedo, "Performance of Multistep Finite Control Set Model Predictive Control for Power Electronics," *Power Electronics, IEEE Transactions on*, vol. 30, no. 3, pp. 1633–1644, 2015.

[16] M. Grötschel, L. Lovász, and A. Schrijver, *Geometric algorithms and combinatorial optimization*. Springer Science & Business Media, 2012, vol. 2.

[17] M. Ajtai, "The shortest vector problem in l 2 is np-hard for randomized reductions," in *Proceedings of the thirtieth annual ACM symposium on Theory of computing*. ACM, 1998, pp. 10–19.

[18] M. O. Damen, K. Abed-Meraim, and M. S. Lemdani, "Further Results on Speeding up the Sphere Decoder," in *Acoustics, Speech and Signal Procesing, 2006 IEEE International Conference on*, Toulouse, May 2006, p. IV.

[19] U. Fincke and M. Pohst, "Improved methods for calculating vectors of short length in a lattice, including a complexity analysis," *Mathematics of computation*, vol. 44, no. 170, pp. 463–471, 1985.